The Astrophysical Journal, 749:103 (9pp), 2012 April 20 doi:10.1088/0004-637X/749/2/103

ENERGETIC PARTICLE DIFFUSION IN STRUCTURED TURBULENCE

T. Laitinen, S. Dalla, and J. Kelly
Jeremiah Horrocks Institute, University of Central Lancashire, PR1 2HE Preston, UK
Received 2011 December 15; accepted 2012 February 10; published 2012 March 27

ABSTRACT

In the full-orbit particle simulations of energetic particle transport in plasmas, the plasma turbulence is typically described as a homogeneous superposition of linear Fourier modes. The turbulence evolution is, however, typically a nonlinear process, and, particularly in the heliospheric context, the solar wind plasma is inhomogeneous due to the transient structures, as observed by remote and in situ measurements. In this work, we study the effects of the inhomogeneities on energetic particle transport by using spatially distributed, superposed turbulence envelopes. We find that the cross-field transport is significantly reduced, when compared to the results obtained with homogeneous turbulence. The reduction can reach an order of magnitude when the enveloping breaks the wave phase coherence along the mean magnetic field direction.

Key words: cosmic rays – diffusion – turbulence

1. INTRODUCTION

When studying solar energetic particle (SEP) events, it is crucial to uncover the propagation of the particles in the interplanetary medium. Energetic particles related to solar eruptions are observed at a large range of latitudes and longitudes (e.g., Dalla et al. 2003; Liu et al. 2011), and without understanding the propagation of particles across the mean magnetic field, it is difficult to determine the extent of the acceleration region and its relation to the physics of the eruption.

The modeling of cosmic-ray transport in turbulent plasmas is typically based on the diffusion–convection equation (Parker 1965) and the quasilinear approach incorporating pitch angle diffusion description, with the cross-field propagation described as field line random walk (Jokipii 1966). The modeling of pitch angle evolution has evolved to include adiabatic focusing (Earl 1976), adiabatic deceleration (Ruffolo 1995; Kocharov et al. 1998), and structured solar wind (Kocharov et al. 2009). The application of these models to obtaining the SEP injection close to the Sun from the observations at 1 AU mostly concentrated on the particle propagation along the mean magnetic field (e.g., Laitinen et al. 2000; Dröge 2003). Only recently has the cross-field propagation been included into the SEP studies (e.g., Zhang et al. 2009; Dröge et al. 2010; He et al. 2011).

A wide range of values for the perpendicular diffusion coefficient has been reported. Studies of the transport of galactic cosmic rays (e.g., Burger et al. 2000) and Jovian electrons (Zhang et al. 2007 and references therein) give estimates of the order of $\kappa_\perp/\kappa_\parallel = 0.01$. On the other hand, Zhang et al. (2003) report values of $\kappa_\perp/\kappa_\parallel = 0.25$ in relation to protons originating from a solar event, while Dwyer et al. (1997) find the ratio to be of the order of unity for energetic particles observed in association with corotating interaction regions.

The values of $\kappa_\perp/\kappa_\parallel$ obtained from observations are related to different regions in the heliosphere, and possibly to different properties of the turbulence, which poses a problem when comparing them with theoretical work. In recent years, the use of full-orbit simulations of energetic particles in studying particle propagation has gained attention. The benefit of this approach is that the parameters defining the turbulence properties can be explicitly prescribed. In addition, for the energetic particle propagation no a priori assumptions, such as the applicability of the diffusion description, are required. The approach has been used by Giacalone & Jokipii (1999), who obtained $\kappa_\perp/\kappa_\parallel = 0.01$–$0.03$, with the perpendicular diffusion coefficient contradicting the quasilinear theory results of Jokipii (1966). Qin et al. (2002) used the method to discover the subdiffusion phase in the particle propagation perpendicular to the mean magnetic field, followed by subsequent recovery of diffusion. This phenomenon has subsequently been modeled as interplay between parallel and perpendicular propagation effects (Matthaeus et al. 2003). Thus, the full-orbit particle simulations have proved to be a valuable tool when studying particle transport.

The full-orbit particle simulation results may depend, however, on the way the turbulent electric and magnetic fields are described. A popular choice is to superpose Fourier modes on a constant magnetic field (e.g., Giacalone & Jokipii 1999; Qin 2002; Qin et al. 2002; Zimbardo et al. 2006; Ruffolo et al. 2008), or more recently, on a Parker spiral field (Tautz et al. 2011). In this approach, however, the modes remain linear throughout the simulation domain, while the heliospheric plasma is known to evolve nonlinearly in addition to linear mode propagation (see, e.g., Tu & Marsch 1995, for a review). Thus, the Fourier-mode description is not consistent with the behavior of plasma turbulence, and using the approach may result in inaccurate particle diffusion coefficients. Some work exists on simulating particles in turbulent fields obtained by using MHD simulations, where the nonlinear interactions are properly addressed (e.g., Beresnyak et al. 2011). However, such studies are limited by computational requirements to a small range of scales and to Cartesian geometries with constant background fields.

The assumption that the plasma turbulence is spatially homogeneous, while useful when comparing the simulations to theoretical models, can also pose a problem when trying to understand SEP observations. The heliospheric magnetic field expands as a Parker spiral and may have a complicated structure (e.g., Parker 1958; Fisk 1996; Sternal et al. 2011). The solar wind is permeated by transient structures, as shown by in situ and remote-sensing observations (Rouillard et al. 2010a, 2010b), thus making it a spatio-temporally varying medium, instead of a steady solar wind flow. Thus, for SEP analysis there is a need to understand how such a structured plasma environment influences energetic particle propagation.

In this work, we study the effect of structures in the turbulence on energetic particle propagation by means of full-orbit energetic particle simulations. We describe the turbulence as a

superposition of localized, randomly distributed envelopes that contain a sum of linear waves. For simplicity, the envelopes are not limited in the direction perpendicular to the mean field, but the variation takes place only along the mean field direction. We introduce two different models to study the effects of the structures. In the *modulated wavefield* model, only the amplitude of the turbulence is modulated, with the individual Fourier modes remaining coherent throughout the simulation domain. In the *random envelope* model, the phases, wave normal directions, and polarizations of the modes are different in different envelopes. This is done to mimic the nonlinear evolution of turbulence being convected throughout the heliosphere. Of these two models, the random envelope model better captures the influence of nonlinear interactions present in the heliospheric turbulence. Comparing the results of the random envelope model with those of the modulated wavefield model allows us to distinguish between the effects of amplitude modulation on one hand, and the phase, wave normal, and polarization changes on the other, as both effects are present in the random envelope model.

The turbulence is superposed on a constant background magnetic field. While such a background field limits the applicability of the model results to the heliospheric environment, it is useful as a first approach in isolating the energetic particle transport effects due to the structured turbulence. The effects of a spatially non-uniform heliospheric magnetic field, and of fully three-dimensional structures, will be the subject of future studies.

In Section 2, we introduce our description of the structured turbulence and our approach to obtain the energetic particle diffusion coefficients. In Section 3, we present the turbulence characteristics, and the full-orbit particle simulations and the derived diffusion coefficients, and study their variation with envelope characteristics, which can be considered as a measure for the structure size in the turbulent plasmas. We discuss the implications of the results and draw our conclusions in Section 4.

2. MODEL

2.1. Turbulence Model

The turbulence model consists of envelopes containing fluctuating magnetic field given by a sum of infinite plane waves. The magnetic field is defined as

$$\mathbf{B} = \mathbf{B}_0 \hat{e}_z + \delta\mathbf{B}(x, y, z),$$

where the background magnetic field is uniform and constant, with $B_0 = 5$ nT, consistent with the magnetic field at 1 AU. The fluctuating field $\delta\mathbf{B}$ is based on the homogeneous turbulence model of Giacalone & Jokipii (1999), and is defined as a sum of N modes,

$$\delta\mathbf{B}(x, y, z) = \sum_{n=1}^{N} A(k_n)\hat{\xi}_n \exp\{i(k_n z'_n + \beta_n)\}. \quad (1)$$

Here $\hat{\xi}_n$ is the polarization vector,

$$\hat{\xi}_n = \cos\alpha_n \hat{\mathbf{x}}'_n + i \sin\alpha_n \hat{\mathbf{y}}'_n.$$

The unprimed coordinate system has the background magnetic field along the z-axis, and the primed coordinate system is obtained from the unprimed through rotation characterized by the spherical coordinate system angles θ_n and ϕ_n of the wave vector $\mathbf{k}_n$, as defined in Giacalone & Jokipii (1999). The fluctuation amplitude $A(k_n)$ is given by a power-law spectrum

$$A^2(k_n) = B_1^2 \frac{G_n}{\sum_{n=1}^{N} G_n}, \quad G(k_n) = \frac{\Delta V_n}{1 + (k_n L_c)^{\gamma}},$$

where B_1^2 is the variance of the magnetic field, L_c is the spectrum's turnover scale, γ is the spectral index, and ΔV_n specifies the volume element in k-space that the discrete mode k_n represents. For the turnover scale, also called the correlation length, we use $L_c = 2.15\, r_\odot$, where $r_\odot$ is the solar radius.

In our simulations, we use the composite spectrum model, which is composed of a sum of slab and two-dimensional (2D) turbulence (Gray et al. 1996). For the slab component, $\mathbf{k}_n$ is directed along the background field, which is parallel to the z-axis, and the polarization vector lies in the xy-plane, with a random polarization angle α_n. For the 2D-component, $\mathbf{k}_n$ lies in the xy-plane. The polarization vector is also in the xy-plane, with $\alpha_n = \pi/2$, perpendicular to $\mathbf{k}_n$, to satisfy $\nabla \cdot \mathbf{B} = 0$. The azimuthal angle ϕ_n and the random phase β_n are chosen from a uniform random distribution.

The slab and 2D spectra have the same turnover scale, and the wavemodes are generated for the same wavenumbers k_n. The wavenumbers are logarithmically spaced between $2\pi/1$ AU and $2\pi/10^{-4}$ AU. The spectral indices for the slab and 2D components are $5/3$ and $8/3$, respectively, and the factor ΔV_n is Δk_n for the slab component and $2\pi k_n \Delta k_n$ for the 2D component. The total turbulence energy is divided between the slab and 2D components with a ratio of 20%:80%, following Bieber et al. (1996).

2.2. Turbulence Envelope Model

We envelope the infinite plane waves, given by Equation (1), into N_p wave packets of length L_p, randomly distributed in the simulation box. The envelopes are of cosine shape, given by

$$\mathfrak{A}_i(z) = \frac{1}{2}\left[1 - \cos\left(2\pi \frac{z - z_i}{L_p}\right)\right] \cdot [\Theta\{z - z_i\} - \Theta\{z - (z_i + L_p)\}], \quad (2)$$

with z_i being the starting point of the envelope, and the Heaviside functions $\Theta\{z\}$ limit each envelope to the range $z_i < z < z_i + L_p$. The magnetic field in these envelopes remains divergence-free, as the envelope amplitude changes only in the direction perpendicular to the polarization vectors $\hat{\xi}_n$. The overall turbulent magnetic field is the sum of the magnetic field in the envelopes,

$$\delta\mathbf{B}(x, y, z) = \sum_{i=1}^{N_p} \mathfrak{A}_i(z)\, \delta\mathbf{B}_i, \quad (3)$$

where $\delta\mathbf{B}_i$ is given by Equation (1). The distribution and summing of the envelopes is shown in the bottom panels of Figure 1, where the gray-filled curves show the amplitudes of each envelope, and the thick curve their sum.

The envelopes are spread randomly along the z-direction from $z = 0$ to $z = L_{\max}$, where the length of the simulation volume along the z-axis, $L_{\max}$, is chosen to be large enough that the particles will remain in the volume for the duration of the simulation. As the variation of the amplitudes takes place only in the z-direction, there is no need to limit the volume in the xy-plane. The number of the envelopes, N_p, is determined by defining an envelope density $\rho_p = N_p L_p / L_{\max}$, which describes the filling of the simulation space with the turbulent envelopes.

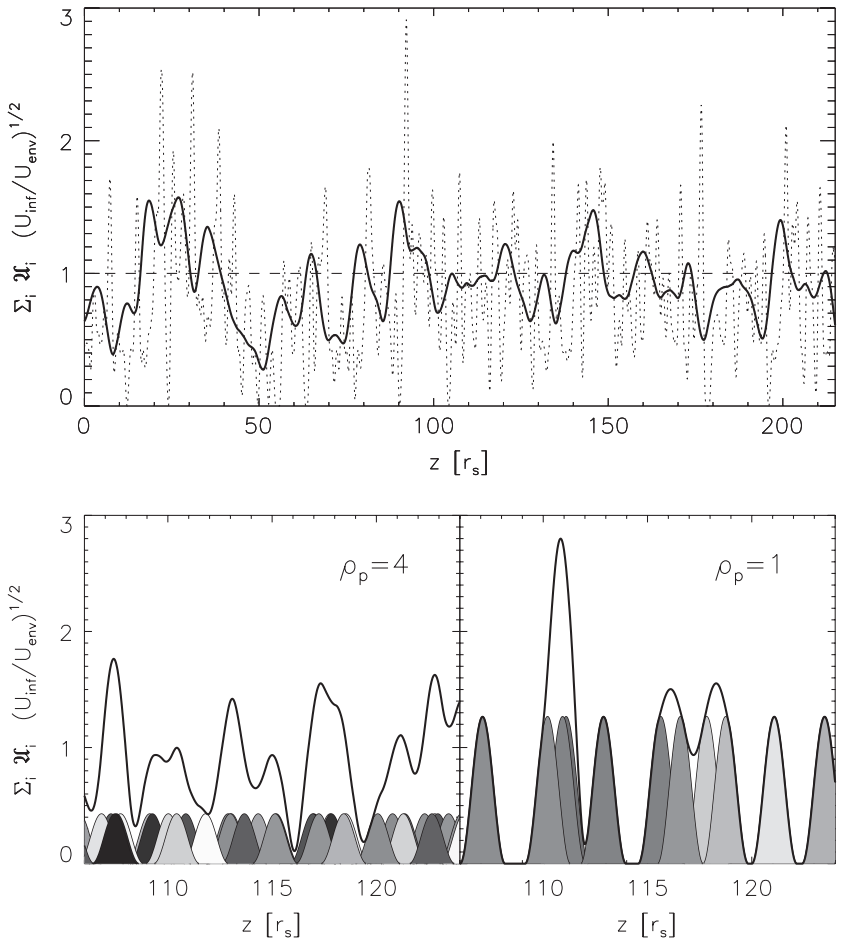

Figure 1. Top panel: the sum of envelope amplitudes for parameters $\rho_p = 16$ and $L_p = 4L_c$ (solid curve), and $\rho_p = 4$ and $L_p = 1L_c$ (dotted curve), in the modulated wavefield model. The horizontal dashed line represents the homogeneous model. Here, the energy density scaling factor $4/\rho^2$ has been used. Bottom panels: the curves filled with gray-scale colors show the individual envelopes with $L_p = L_c$. The thick curve represents the sum of the envelopes.

We consider two different models for $\delta\mathbf{B}_i$. In the *wavefield modulation* model, the set of angles β_n, ϕ_n, and α_n are the same for each envelope, and thus the enveloping only modulates the turbulent field described by Equation (1). In the *random envelope* model, each envelope i has a unique set of angles $\beta_{\rm ni}$, $\phi_{\rm ni}$, and $\alpha_{\rm ni}$, mimicking the spatial evolution of the turbulence phases and wavenumbers.

2.3. Turbulence Energy Density

To compare the turbulent fields and their effects on SEP propagation, we scale the fluctuation amplitudes so that the average energy density in the fluctuating field is independent of the enveloping parameters. As the energy density varies considerably in the enveloped cases, we calculate the energy density over a large spatial domain. The average energy density in a volume of cross-section S and height $L_{\rm max}$ is given by

$$U = \frac{1}{8\pi}\frac{1}{S\ L_{\rm max}}\int\int \delta B^2 dz\ dS = \frac{1}{8\pi}\langle \delta B^2\rangle,$$

where $\langle \delta B^2\rangle$ is the variance of the fluctuations over the volume. The energy density for the enveloped turbulence is then

$$U_{\rm env} = \frac{1}{8\pi\, L_{\rm max}}\int_0^{L_{\rm max}} \sum_{i=1}^{N_p}\sum_{j=1}^{N_p} \mathfrak{A}_i\mathfrak{A}_j \delta\mathbf{B}_i\cdot\delta\mathbf{B}_j\ dz. \quad (4)$$

For the random envelope model, this integral can be estimated analytically (see the Appendix). For the wavefield modulation model, the scaling factor is obtained through numerical integration.

2.4. Energetic Particle Simulations

In order to study charged particle propagation in turbulent magnetic fields, we integrate the fully relativistic equation of motion of energetic protons using the simulation code by Dalla & Browning (2005). As the fluctuating field is magnetostatic, the electric field is zero. For the integration, we use the Bulirsh–Stoer method (Press et al. 1993). The method uses adaptive timestepping to control the accuracy by limiting the error between consecutive steps to a given tolerance. We use the tolerance of 10^{-9}, which ensures the conservation of energy to within 10^{-6} in our simulations. The particles' initial velocity distribution is isotropic and monoenergetic, and their initial positions are selected randomly in a region 40 times the size of the turbulence correlation scale, in order to minimize the effects of the local magnetic field. For each set of turbulence and particle parameters, we run the simulations for 10 field realizations, with 2048 particles for each simulation. In the turbulence realizations, we typically use $N = 128$ Fourier modes, with validation runs using $N = 1024$ modes to verify that the results are not altered by the number of modes.

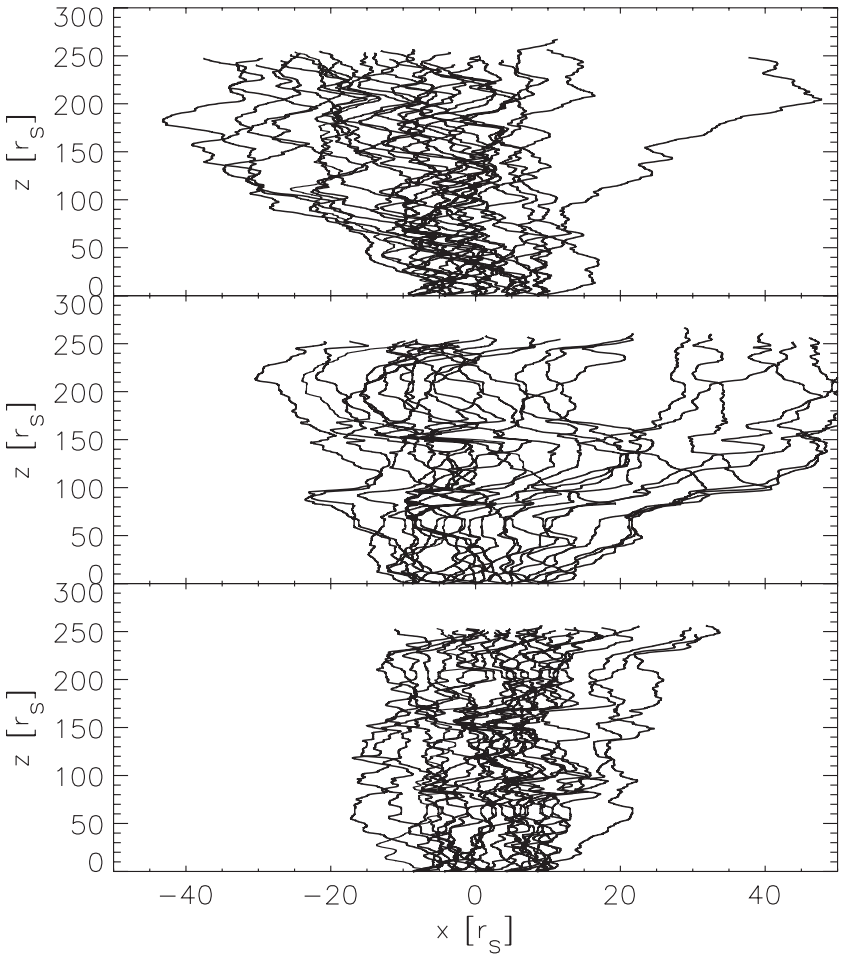

Figure 2. Field lines in the homogeneous (top panel), modulated wavefield (middle panel), and the random envelope turbulence model (bottom panel). In the latter two models, the envelope length is $L_p = 4L_c$ and density $\rho_p = 4$.

The diffusion coefficient is obtained from the definition

$$\kappa_{\zeta\zeta} = \frac{\langle \Delta\zeta^2 \rangle}{2t}, \quad \zeta = x, y, z \tag{5}$$

(e.g., Giacalone & Jokipii 1999), where the square of the displacement, $\Delta\zeta^2$, is averaged over the simulated particles. The diffusion coefficients are calculated separately for each field realization. In Figures 4–6, $\kappa_{\rm par}$ refers to κ_{zz}, whereas $\kappa_{\rm perp}$ is obtained as the mean of κ_{xx} and κ_{yy}.

The diffusion coefficients experience typically super- and subdiffusive phases, after which they settle to constant values, which we use in this study. In practice, we continue the simulations to ∼100 parallel diffusion times in each run. In addition to this, we require that the particles be spread over a large number of envelopes. For this, we require that the FWHM of the distribution, as calculated from the analytic solution to the diffusion equation (e.g., Giacalone & Jokipii 1999), $4\sqrt{\kappa_{zz} t \ln 2}$, is at least $40L_p$. This is done in order to reduce the statistical errors caused by the local differences between different field realizations.

We have reproduced some of the simulations done by Giacalone & Jokipii (1999), and found good agreement with their example run presented in their Appendix A. We found, however, that the agreement between their experiments one and three is somewhat dependent on the selection of simulation domain size and fitting parameters when using experiment one. For this reason, the results presented in this study may differ somewhat from their results, as they use experiment one for their results, whereas our method corresponds to their experiment three.

The diffusion of the particles can be caused by field line meandering and by the drifts of the particles relative to the field lines. However, these processes are strongly coupled. Even a small drift of a particle from its original field line can result in large deviation from the original field line, depending on the local structure of the magnetic field. For this reason, separating the contributions of the two effects is not trivial. In this study, we do not attempt to make this distinction, but consider the diffusion as a compound effect of the two processes.

3. RESULTS

In this work, we study the effect of turbulent structures on energetic particle transport by using the turbulence model described in Section 2, varying the enveloping parameters. For the envelope density ρ_p we have chosen to use values 1, 4, and 16, to represent tenuous to dense enveloping. The length of the envelope, L_p, is chosen to have values L_c, 4 L_c, and 16 L_c. In this section, we first study how the enveloping affects the turbulence, and then how the particle propagation is affected.

3.1. Enveloped Turbulent Field

To understand how the enveloping affects the turbulence, it is useful to compare the behavior of the envelope amplitudes to the homogeneous turbulence. In the top panel of Figure 1

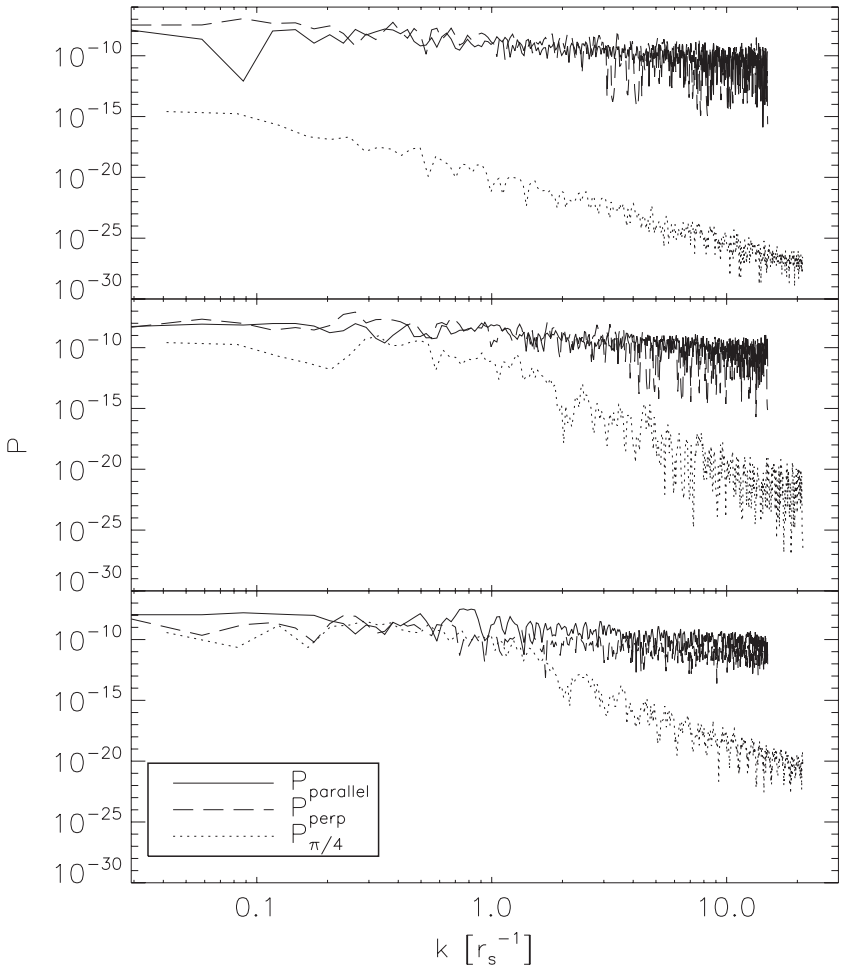

Figure 3. Power spectrum of the turbulence using the homogeneous (top panel), modulated wavefield (middle panel), and the random envelope turbulence model (bottom panel). In the latter two models, the envelope length is $L_p = 4L_c$ and density $\rho_p = 4$.

we plot the sum of the envelope amplitudes for the wavefield modulation model, for two combinations of ρ_p and L_p. As can be seen, the high-density enveloping, with $\rho_p = 16$, results in smaller deviations from the homogeneous model (the horizontal dashed curve) than the intermediate density ($\rho_p = 4$). Thus, the envelope density describes the strength of the deviation of the mean amplitude from a constant value. The tenuous enveloping, with $\rho_p = 1$ (bottom right panel of Figure 1), implying an average of one envelope at a given position, results in regions with no turbulence at all and regions with overlapping envelopes. While such a situation is not necessarily realistic, it is taken as an extreme of the parameterization and can, in later studies, be more realistically supplemented with some small underlying homogeneous turbulence. At the large density limit, the wavefield modulation approaches the homogeneous turbulence description.

We can also visualize how the field line wandering is affected by the enveloping. Figure 2 shows the field lines for homogeneous turbulence (top panel), the modulated wavefield (middle panel), and the random envelope model (bottom panel), for parameters $L_p = 4L_c$ and $\rho_p = 4$. The field lines are initiated from an area of $10L_c \times 10L_c$ at $z = 0$. The most striking difference can be seen in the reduced spreading of the field lines in the case of random enveloping (bottom panel of Figure 2). There are also some qualitative differences between the homogeneous and modulated wavefield models (the top and middle panels). However, they cannot be quantified on the basis of one realization, and we will study their difference by using the energetic particle simulations in Section 3.2.

It is also important to determine how the turbulence spectrum is affected by enveloping. This can be seen in Figure 3, where we present 2D Fourier transforms of the turbulence for the homogeneous (top panel), the modulated wavefield (middle panel) and the random envelope turbulence model (bottom panel). We show the spectrum for waves with the k along the mean magnetic field (solid line), along an axis perpendicular to it (dashed line), and along the direction 45° away from the mean magnetic field (dotted line). It can be seen that for the homogeneous turbulence the wave power resides in the parallel and perpendicular components only, whereas the enveloping effectively isotropizes the turbulence at scales larger than the envelope length ($L_p = 4L_c$). In the random envelope model, the perpendicular component of the spectrum (the dashed line in the bottom panel of Figure 3) is reduced compared to the two other models. This may have an influence on energetic particle transport.

It should be noted that in this section we have presented the behavior of the amplitudes, field lines and spectra for only one realization, and one region. Thus, the presented behavior can only be considered as qualitative, as localized structures are apparent even in homogeneous turbulence models (e.g., Chuychai et al. 2007).

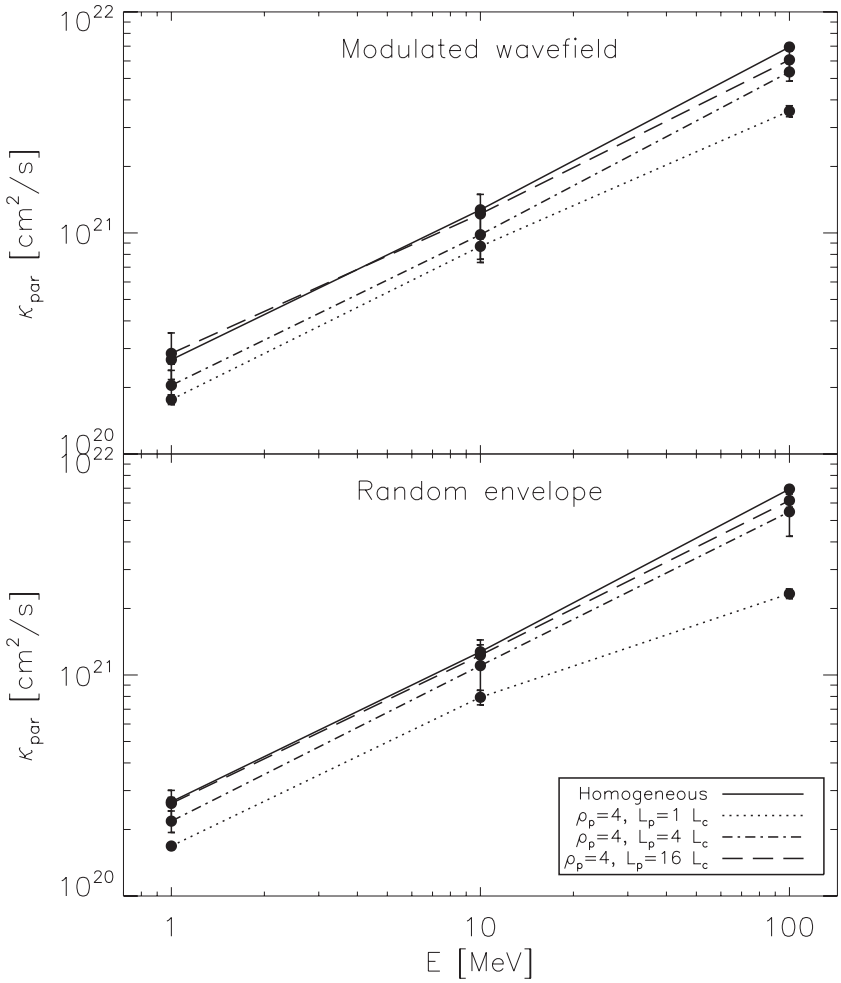

Figure 4. Parallel diffusion coefficient as a function of particle energy, for the modulated wavefield model (top panel) and for the random envelope model (bottom panel), for $\rho_p = 4$ and four envelope lengths. The solid line represents the result for homogeneous turbulence. The turbulence amplitude is $B_1^2/B_0^2 = 1$.

3.2. Energetic Particle Propagation

To study the influence of enveloping the turbulence on energetic particle propagation, we have simulated several different scenarios, varying the particle energy and the turbulence properties. In Figure 4, we show the parallel diffusion coefficients obtained from these runs, for protons of energies 1 MeV, 10 MeV, and 100 MeV. The points represent the mean, and the error limits the standard deviation of the diffusion coefficients, obtained from 10 turbulence realizations. The top panel shows the modulated wavefield results and the bottom one those of the random envelope model.

In both panels of Figure 4, the solid black line depicts the diffusion coefficient obtained from runs with homogeneous turbulence, given by Equation (1), which are consistent with the results of Giacalone & Jokipii (1999). The non-solid lines show the parallel diffusion coefficient for enveloped turbulence, with intermediate envelope density ($\rho_p = 4$) and three envelope lengths. The enveloping reduces the diffusion coefficients somewhat for the modulated wavefield model up to factor of two compared to the homogeneous turbulence model (top panel) and the random envelope model up to factor of three (bottom panel), and has a dependence on the envelope length.

For the perpendicular diffusion coefficient, the effect of the enveloping is more varied. In Figure 5, we show the variation of the perpendicular diffusion coefficient as a function of energy for the same parameters as in Figure 4. In the modulated wavefield model, the perpendicular diffusion coefficient is reduced by a factor of two compared to the homogeneous turbulence result and is independent of the envelope length. For the random envelope model, the reduction is strongly dependent on the envelope length, and the reduction in the diffusion coefficient reaches a factor of eight for short envelopes.

The effect of the enveloping parameters can be seen in more detail in Figure 6, where we show the perpendicular diffusion coefficient for three envelope densities, as a function of the envelope length. For the modulated wavefield model (top panel), there is no variation of the perpendicular diffusion with the envelope length, within statistical errors of our study. There is a clear dependence on the envelope density, however, with a reduction of the diffusion coefficient up to factor of three compared to the homogeneous turbulence result, when the turbulence enveloping is tenuous ($\rho_p = 1$ in the top panel of Figure 6). Higher envelope densities result in the diffusion coefficient approaching the homogeneous turbulence values.

When the phases, propagation directions, and polarizations are different from one envelope to another, the cross-field particle propagation depends considerably on both enveloping parameters (bottom panel of Figure 6). For a high-density, long-envelope packeting, the limit of homogeneous turbulence is again obtained. When the envelopes are shortened and

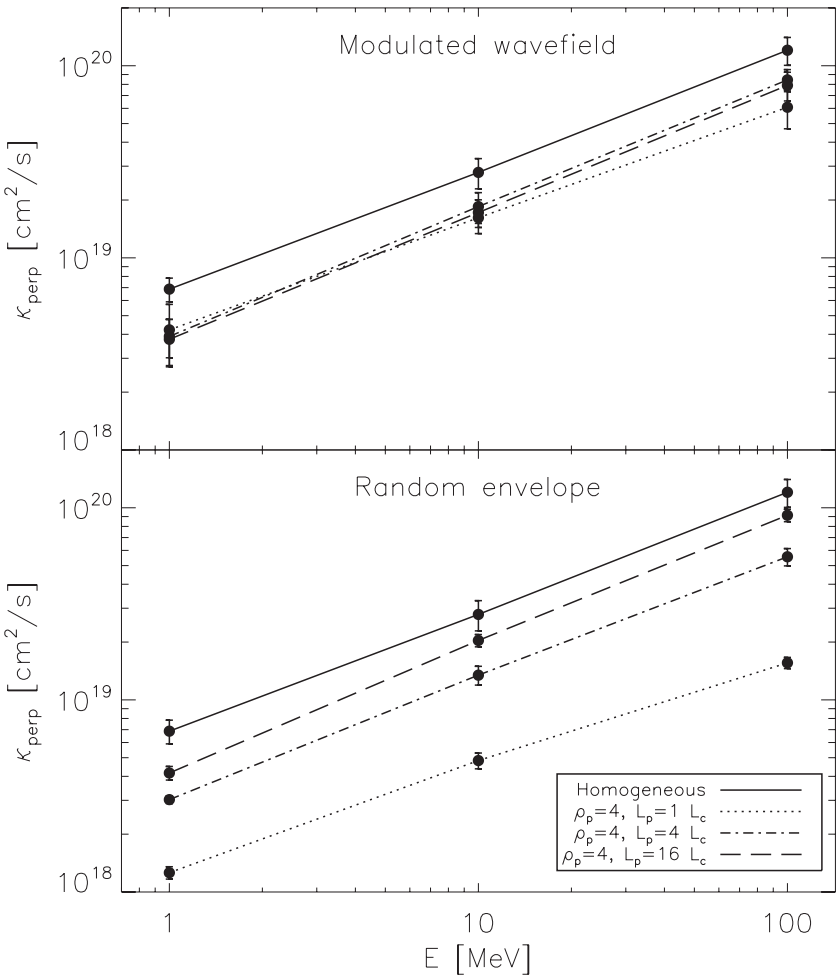

Figure 5. Perpendicular diffusion coefficient as a function of energy, for the modulated wavefield model (top panel) and for the random envelope model (bottom panel). The turbulence amplitude is $B_1^2/B_0^2 = 1$.

the envelope density is reduced, however, the reduction of the perpendicular diffusion coefficient is nearly an order of magnitude.

4. DISCUSSION AND CONCLUSIONS

In this work, we have studied the effect of structured turbulence, as opposed to homogeneous turbulence, on energetic particle transport. We find that in the structured turbulence the particle propagation is significantly inhibited, as compared to the propagation in homogeneous turbulence of similar mean energy density of the turbulent magnetic field.

The parallel diffusion can be seen to be affected strongly only when the inhomogeneities are of small scales (the dotted curve in Figure 4). The reduction of the coefficient also has a significant energy dependence, with higher-energy particles being affected more strongly. This may be related to the increasing resonant scales of the particles (with Larmor radius of 0.4 $r_\odot$ for 100 MeV protons in a 5 nT magnetic field).

The effect of the structuring of the turbulence on the cross-field propagation depends strongly on how the enveloping is performed. In the modulated wavefield model, where only the amplitude of the turbulence is modified, the cross-field propagation is sensitive only to the envelope density. For short envelopes, it appears that the effect of reduced field line wandering in the regions with small-amplitude turbulence is not fully compensated by the increased wandering in the higher-amplitude regions, but overall the cross-field propagation is inhibited. With the increase of the envelope density, the variation of the turbulence amplitudes approaches the homogeneous description (see Figure 1), and the limit of cross-field propagation in the homogeneous turbulence is approached with increasing envelope density, as can be seen in the top panel of Figure 6.

For the random envelope model, however, the effect of the enveloping to the cross-field propagation is more varied, and stronger, and both the length and the density affect the perpendicular diffusion coefficient. Thus, the loss of phase coherence along the mean field direction, which is the basic difference between the wavefield modulation and random envelope models, significantly affects the cross-field propagation of energetic particles.

This effect can be understood qualitatively. Strong cross-field wandering of a field line, as seen in the top panels of Figure 2, can only take place due to persistent cross-field disturbance with little or no dependence on the coordinate along the background magnetic field. This is possible due to the 2D component of the turbulence: a 2D wave has a constant phase along the background magnetic field and the cross-field direction perpendicular to the k-vector. In the homogeneous and modulated wavefield model such waves are coherent throughout the simulation region (subject to disturbances from other waves), resulting in strong wandering of some field lines. In the random envelope model, however, this coherence is broken, and

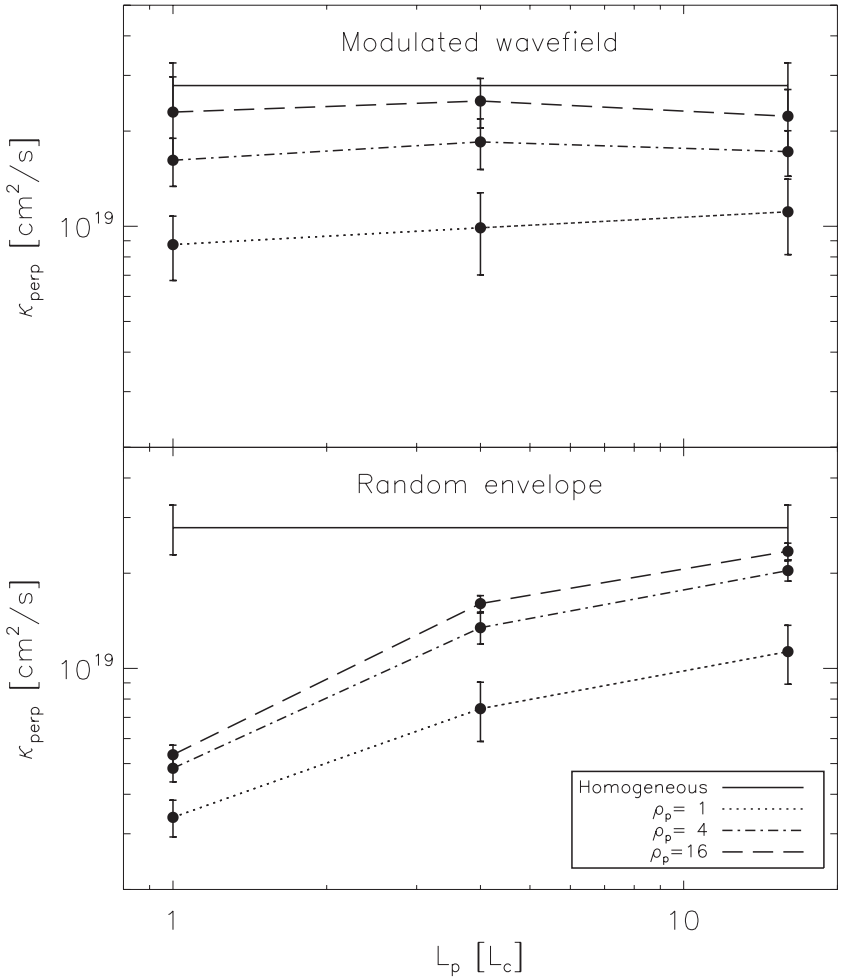

Figure 6. Perpendicular diffusion coefficient as a function of the envelope length for the modulated wavefield model (top panel) and for the random envelope model (bottom panel). The turbulence amplitude is $B_1^2/B_0^2 = 1$ and the particle energy 10 MeV.

such wandering can remain coherent only when one envelope dominates the others.

Such breaking of the behavior has natural justifications, particularly in the heliospheric context. As discussed in Section 1, the heliospheric magnetic field, and thus the turbulence, has its origins at the Sun, and the heliospheric plasmas are known to be structured due to transient phenomena at the Sun. Thus, it does not seem feasible that the evolving corona could produce structures with infinite phase coherence into the heliospheric magnetic fields.

The nonlinear evolution of turbulence also favors the evolution of the turbulence in a parallel direction. As waves propagate outward from the Sun, they interact nonlinearly, resulting in a cascade of energy between different scales (e.g., Tu & Marsch 1995). Although this energy cascade is very anisotropic, toward small perpendicular scales, the parallel scales are also affected. This can be understood through the concept of critical balance, introduced by Goldreich & Sridhar (1995), where the turbulence separated by the critical scale parallel to the mean field experience differing interactions due to the evolution of the counterstreaming waves. This results in scale-dependent anisotropy between the perpendicular and parallel scales of the turbulence, which has been observed in the solar wind turbulence (Horbury et al. 2008).

Overall, our results suggest that inhomogeneities within heliospheric plasmas and the nonlinear behavior of the turbulence may significantly influence energetic particle transport. This has significant implications on the studies of SEP origins and their propagation in the heliospheric magnetic fields.

We acknowledge support from the UK Science and Technology Facilities Council via standard grant ST/H002944/1 and a PhD studentship. Access to the University of Central Lancashire's High Performance Computing Facility is gratefully acknowledged.

APPENDIX

CALCULATION OF THE MEAN TURBULENCE ENERGY DENSITY

For the random envelope model, the energy density given by Equation (4) can be estimated analytically. As the magnetic fields $\delta\mathbf{B}_i$ within different envelopes are not correlated, we can consider the integral over terms with $i \neq j$ negligible. With this approximation, the integral can be written in the form

$$U_{\rm env} = \frac{1}{8\pi}\frac{1}{L_{\rm max}S}\sum_{i=1}^{N_p}\int_0^{L_{\rm max}} \delta B_i^2 \mathfrak{A}_i(z)^2 \, dz \, dS.$$

Using $\delta B^2(x, y, z) \approx \langle \delta b^2 \rangle$ on the scales where $\mathfrak{A}_i$ changes appreciably, and ignoring the envelopes that are only partly in

the integration region, the integral results in

$$U_{\rm env} = \frac{3}{8}\frac{L_p}{L_{\rm max}} U_{\rm inf},$$

where $U_{\rm inf}$ is the energy density of the turbulence given by Equation (1). Thus, the scaling factor for the enveloped turbulence energy density is

$$\frac{U_{\rm inf}}{\sum_{N_p} U_{\rm env}} = \frac{8}{3}\frac{L_{\rm max}}{N_p L_p} = \frac{8}{3\rho_p}.$$

The magnetic field amplitude is scaled by the square root of this scaling factor. We have verified the validity of this estimate through numerical integration of δB^2.

For the wavefield modulation model, the amplitudes can simply be added together, as the wave phases and polarizations are the same in all envelopes. At high envelope density, the sum approaches constant, thus the scaling factor for the energy density is simply $4/\rho_p^2$. On the limit of low envelope density, the envelopes do not overlap, resulting in the same expression for the energy density as in the random envelope model, and the scaling factor $8/(3\rho_p)$. However, as the envelope densities in this study are in the intermediate range between these asymptotes, we use numerical integration for determining the scaling factor in the wavefield modulation model.

REFERENCES

Beresnyak, A., Yan, H., & Lazarian, A. 2011, ApJ, 728, 60
Bieber, J. W., Wanner, W., & Matthaeus, W. H. 1996, J. Geophys. Res. (Space Phys.), 101, 2511
Burger, R. A., Potgieter, M. S., & Heber, B. 2000, J. Geophys. Res., 105, 27447
Chuychai, P., Ruffolo, D., Matthaeus, W. H., & Meechai, J. 2007, ApJ, 659, 1761
Dalla, S., & Browning, P. K. 2005, A&A, 436, 1103
Dalla, S., Balogh, A., Krucker, S., et al. 2003, Ann. Geophys., 21, 1367
Dröge, W. 2003, ApJ, 589, 1027
Dröge, W., Kartavykh, Y. Y., Klecker, B., & Kovaltsov, G. A. 2010, ApJ, 709, 912
Dwyer, J. R., Mason, G. M., Mazur, J. E., et al. 1997, ApJ, 490, L115
Earl, J. A. 1976, ApJ, 205, 900
Fisk, L. A. 1996, J. Geophys. Res., 1011, 15547
Giacalone, J., & Jokipii, J. R. 1999, ApJ, 520, 204
Goldreich, P., & Sridhar, S. 1995, ApJ, 438, 763
Gray, P. C., Pontius, D. H., & Matthaeus, W. H. 1996, Geophys. Res. Lett., 23, 965
He, H.-Q., Qin, G., & Zhang, M. 2011, ApJ, 734, 74
Horbury, T. S., Forman, M., & Oughton, S. 2008, Phys. Rev. Lett., 101, 175005
Jokipii, J. R. 1966, ApJ, 146, 480
Kocharov, L., Pizzo, V. J., Odstrcil, D., & Zwickl, R. D. 2009, J. Geophys. Res. (Space Phys.), 114, A05102
Kocharov, L., Vainio, R., Kovaltsov, G. A., & Torsti, J. 1998, Sol. Phys., 182, 195
Laitinen, T., Klein, K.-L., Kocharov, L., et al. 2000, A&A, 360, 729
Liu, Y., Luhmann, J. G., Bale, S. D., & Lin, R. P. 2011, ApJ, 734, 84
Matthaeus, W. H., Qin, G., Bieber, J. W., & Zank, G. P. 2003, ApJ, 590, L53
Parker, E. N. 1958, ApJ, 128, 664
Parker, E. N. 1965, Planet. Space Sci., 13, 9
Press, W. H., Teukolsky, S. A., Vetteling, W. T., & Flannery, B. P. 1993, Numerical Recipes in Fortran: The Art of Scientific Computing (2nd ed.; New York NY: Cambridge Univ. Press)
Qin, G. 2002, PhD thesis, Univ. Delaware
Qin, G., Matthaeus, W. H., & Bieber, J. W. 2002, ApJ, 578, L117
Rouillard, A. P., Davies, J. A., Lavraud, B., et al. 2010a, J. Geophys. Res. (Space Phys.), 115, 4103
Rouillard, A. P., Lavraud, B., Davies, J. A., et al. 2010b, J. Geophys. Res. (Space Phys.), 115, 4104
Ruffolo, D. 1995, ApJ, 442, 861
Ruffolo, D., Chuychai, P., Wongpan, P., et al. 2008, ApJ, 686, 1231
Sternal, O., Engelbrecht, N. E., Burger, R. A., et al. 2011, ApJ, 741, 23
Tautz, R. C., Shalchi, A., & Dosch, A. 2011, J. Geophys. Res. (Space Phys.), 116, A02102
Tu, C.-Y., & Marsch, E. 1995, Space Sci. Rev., 73, 1
Zhang, M., Jokipii, J. R., & McKibben, R. B. 2003, ApJ, 595, 493
Zhang, M., Qin, G., & Rassoul, H. 2009, ApJ, 692, 109
Zhang, M., Qin, G., Rassoul, H., et al. 2007, Planet. Space Sci., 55, 12
Zimbardo, G., Pommois, P., & Veltri, P. 2006, ApJ, 639, L91